Plakophilin 3 and Par3 facilitate desmosomes' association with the apical junctional complex

Indrajyoti Indra[a], Regina B. Troyanovsky[a], Kathleen J. Green[b,*], and Sergey M. Troyanovsky[a,*]
[a]Departments of Dermatology and Cell & Molecular Biology and [b]Departments of Pathology and Dermatology, Northwestern University, The Feinberg School of Medicine, Chicago, IL 60611

ABSTRACT **Desmosomes (DSMs), together with adherens junctions (AJs) and tight junctions (TJs), constitute the apical cell junctional complex (AJC). While the importance of the apical and basolateral polarity machinery in the organization of AJs and TJs is well established, how DSMs are positioned within the AJC is not understood. Here we use highly polarized DLD1 cells as a model to address how DSMs integrate into the AJC. We found that knockout (KO) of the desmosomal ARM protein Pkp3, but not other major DSM proteins, uncouples DSMs from the AJC without blocking DSM assembly. DLD1 cells also exhibit a prominent extraDSM pool of Pkp3, concentrated in tricellular (tC) contacts. Probing distinct apicobasal polarity pathways revealed that neither the DSM's association with AJC nor the extraDSM pool of Pkp3 are abolished in cells with defects in Scrib module proteins responsible for basolateral membrane development. However, a loss of the apical polarity protein, Par3, completely eliminates the extraDSM pool of Pkp3 and disrupts AJC localization of desmosomes, dispersing these junctions along the entire length of cell–cell contacts. Our data are consistent with a model whereby Par3 facilitates DSM assembly within the AJC, controlling the availability of an assembly competent pool of Pkp3 stored in tC contacts.**

Monitoring Editor
Thomas Magin
University of Leipzig

Received: Jan 4, 2021
Revised: Jun 22, 2021
Accepted: Jul 1, 2021

INTRODUCTION

The integrity of epithelial tissues depends on the joint activity of three major junctional structures: tight junctions (TJs), adherens junctions (AJs), and desmosomes (DSMs). These junctions exhibit a stereotypical organization along the apical end of the cell lateral membrane: TJs are most apical, followed by AJs and then DSMs (Farquhar and Palade, 1963). Together, these three junction types organize the so-called apical junctional complex (AJC), which defines the boundary between two functionally and structurally distinct cell domains: the apical, facing the lumen, and the basolateral, involved in communication with other cells and the extracellular matrix. The assembly and maintenance of AJs and TJs in the AJC require a signaling network of polarity proteins (reviewed in Tepass *et al.*, 2001; Dow and Humbert, 2007; Goldstein and Macara, 2007; Bonello and Peifer, 2019). Two groups of these proteins, apical polarity proteins (which are subdivided into Crumbs and Par complexes) and basolateral proteins in the Scrib complex, mutually exclude each other from their respective cell domains, thereby maintaining the identity of the apical and basolateral plasma membranes. It is well established that this signaling network directly determines the sites of TJ and AJ assembly. However, in spite of the fact that DSMs are an essential component of the polarized AJC, how these junctions are integrated into and controlled by the apical or basolateral polarity machinery is unknown. In this work we sought to address this gap in our understanding of the relationship between DSMs and polarity signaling.

In addition to polarity proteins, another cytoarchitectural component that coordinates coupling of TJs and AJs is the cortical actomyosin cytoskeleton, which is tightly associated with and plays a key scaffolding role in their formation and maintenance (Campbell *et al.*, 2017; Garcia *et al.*, 2018). In contrast, adhesion receptors of DSMs, desmoglein (Dsg) and desmocollin (Dsc), interact with intermediate filaments (IFs) through the linker protein

This article was published online ahead of print in MBoC in Press (http://www.molbiolcell.org/cgi/doi/10.1091/mbc.E21-01-0001) on July 14, 2021.

*Address correspondence to: Sergey M. Troyanovsky (s-troyanovsky@northwestern.edu); Kathleen J. Green (kgreen@northwestern.edu).

Abbreviations used: ABP, apicobasal polarity; AJ, adherens junction; AJC, apical junctional complex; bC, bicellular; crRNA, CRISPR RNA; Dsc, desmocollin; Dsg, desmoglein; DSM, desmosome; Dsp, dessmoplakin; FPKM, fragments per kilobase of transcript per million; IF, intermediate filament; KO, knockout; PCC, Pearson's correlation coefficient; Pg, plakoglobin; Pkp, plakophilin; PLA, Proximity ligation assay; rDSM, rudimentary desmosome; tC, tricellular; TJ, tight junction.

desmoplakin (Dsp). While this association plays a critical functional role in tissue integrity, DSM-like structures still form in cells lacking IFs or Dsp (Vasioukhin *et al.*, 2001; Sumigray and Lechler, 2012; Bär *et al.*, 2014). Some data suggest that cross-talk between DSMs and other components of AJCs occurs through direct interactions between extracellular regions of Dsg and an AJ adhesive receptor, E-cadherin (Shafraz *et al.*, 2018). How this interaction contributes to initiation of DSM assembly and the extent to which other intracellular DSM protein(s) initiate and support Dsg and Dsc clustering and formation of IF-bound DSM plaques is still poorly understood.

Identification of the intracellular proteins responsible for coordinating desmosomal cadherin clustering with plaque assembly will be critical for untangling the mechanisms of DSM assembly and regulation. Indeed, a loss of function of a key F–actin-binding AJ protein α-catenin completely abolished AJ assembly (Ozawa, 1998; Imamura *et al.*, 1999). DSM assembly, by contrast, is extremely robust—the inactivation of any of the major intracellular DSM proteins or associated keratin IFs, while resulting in clear defects in DSMs, is unable to abolish their formation (reviewed in Holthöfer *et al.*, 2007; Green *et al.*, 2010). Furthermore, clustering of desmosomal cadherins and Dsp appears to precede elaboration of IFs at the plasma membrane (Moch *et al.*, 2020). The only way to abolish DSM formation appears to be the combinatorial knockdown of the DSM plaque proteins plakophilins (Pkp; Todorovic *et al.*, 2014; Fujiwara *et al.*, 2015).

Pkp1, Pkp2, and Pkp3 are important constituents of DSM plaques and belong to the p120 subfamily of the ARM repeat domain proteins. A striking feature of these proteins is their involvement in diverse and apparently distinct processes ranging from regulation of transcription and translation to growth factor signaling (Gerull *et al.*, 2004; Hatzfeld *et al.*, 2014; reviewed in Hofmann, 2020). Evidence supports a role for Pkps in the early stages of DSM plaque precursor assembly as well as in helping link the Dsg- and Dsc-associated protein plakoglobin (Pg) to Dsp (Godsel *et al.*, 2010; Broussard *et al.*, 2015). It was also suggested that Pkps interact with the juxtamembrane region of desmosomal cadherins to promote Dsc clustering (Troyanovsky *et al.*, 1994; Fujiwara *et al.*, 2015). Finally, the role of Pkp1 in Dsg clustering has been suggested by a cross-linking analyses (Fuchs *et al.*, 2019). Altogether, the data support the idea that the combined function of Pkps is crucial for the initial steps of DSM assembly and therefore an important intermediate in the coordinated assembly of the AJC.

Here we use a well-established in vitro model of simple polarized epithelial cells to reveal a mechanism by which desmosomal Pkps cooperate with the classic apical polarity machinery to integrate DSMs into the AJC. We demonstrate that while the joint activity of Pkp2 and Pkp3 is essential for DSM formation, Pkp3 activity is uniquely required to recruit DSMs to the AJC. We also identify a significant extraDSM pool of Pkp3 that is concentrated in the cortex of tricellular (tC) contacts. While the basolateral polarity Scrib module is required for proper localization of the entire AJC, genetic interference with Scrib proteins fails to uncouple DSMs from the AJC or abolish this cortical extraDSM pool of Pkp3. In contrast, the apical membrane identity protein, Par3, is critical for both DSM association with the AJC and concentrating Pkp3 in tC contacts. Altogether, our data uncover a role for classic polarity protein machinery, in association with desmosomal Pkp3, in coordinating DSM assembly into, and maintenance in, the AJC proper. These data fill a gap in our understanding of how these "newest" vertebrate intercellular junctions map onto the more ancient AJ and TJ network.

RESULTS

DSMs of DLD1 cells are organized in AJC-associated linear arrays

Double staining for the AJC and TJ protein component, ZO1, and the DSM protein, Dsg2 (Figure 1A) in the DLD1 colon carcinoma cell line, shows that the spatial organization of DSMs in these cells corresponds to that known for simple epithelia (Farquhar and Palade, 1963). Similar to what was reported in this classic study, the majority of DSMs in DLD1 cells were observed to be arranged in arrays, typically aligned with a single circumferential TJ belt along the apical end of cell lateral membrane. We observed that alignment between the DSM array and the TJs in 2D images can deviate from one another, in some cases, up to several μm (Figure 1A, cell b, arrows). However, analysis of confocal z slices showed that all DSM arrays were located at the apical end of the lateral membrane (marked by an arrow in Figure 1C). This could be appreciated by comparing the cumulative projections of three optical z slices spanning the apical 1.5 μm of the cell membrane ("apical" portion) and remaining slices of the "basal" portion, spanning about 4–6 μm of the basolateral membrane (Figure 1C and Supplemental Figure S1). The majority of DSMs were observed to localize with other components of AJC, TJs, and AJs in the apical portion. The basal portion exhibited either none or just isolated DSMs that are smaller than DSMs detected in the apical portion (see also below). Overall, the majority of DSMs in DLD1 cells were observed to be integrated into the AJC as in epithelial tissues, making these cells a convenient cell culture model to study the process of spatial organization of DSM as well as interdependence of cell–cell junctions in simple epithelia.

Pkp3 contributes to the integration of DSM into AJC

Association of DSMs with AJC suggests that the assembly of these structures is coordinated. To determine the extent to which DSM proteins contribute to coordination mechanisms, we applied the CRISPR-Cas9 genetic approach to create DSM molecule-specific KO lines. To determine which genes to delete, we first carried out RNA-seq analyses of DLD1 cells and found that they express a repertoire of major DSM proteins typical for simple epithelia: Dsg2, Dsc2 (a and b variants), Dsp and Pg (two transcription variants of each), and single transcriptional variants of Pkp2 and Pkp3 (see Figure 2A). Based on these data, we produced four DLD1-KO cell sublines, each lacking an individual member of the identified DSM proteins (Figure 2B). Confocal immunofluorescence microscopy with an anti-Dsg2 antibody showed that all generated cell lines formed bright Dsg2-containing puncta (Figure 3, A and B), referred to below as rudimentary DSMs (rDSMs). This observation indicated that none of the tested proteins are essential for generating Dsg2 clusters, one of the critical steps in DSM assembly. In the Dsp-KO, the rDSMs were obviously smaller than wt DSMs and the level of Dsg2 staining in the membrane outside of rDSMs increased. However, these cells, despite such abnormalities, were able to organize their rDSMs into arrays located at the apex of the lateral membrane. Virtually no rDSMs were present in the remaining "basal" portion of the cells (Figure 3B). The dramatic difference in rDSM numbers and DSM fluorescence intensities along the apicobasal axes in wt DLD1 and Dsp-KO cells was also revealed by quantification of rDSMs through confocal optical slices of 50 × 50 μm imaging fields, each containing up to eight cells (Figure 3, C and D). While the number of rDSMs in the "basal" portion in Pg-KO and in Pkp2-KO cells increased, rDSMs in these cells also showed a clear preference for the most apical regions of the lateral membranes (Figure 3, A–C).

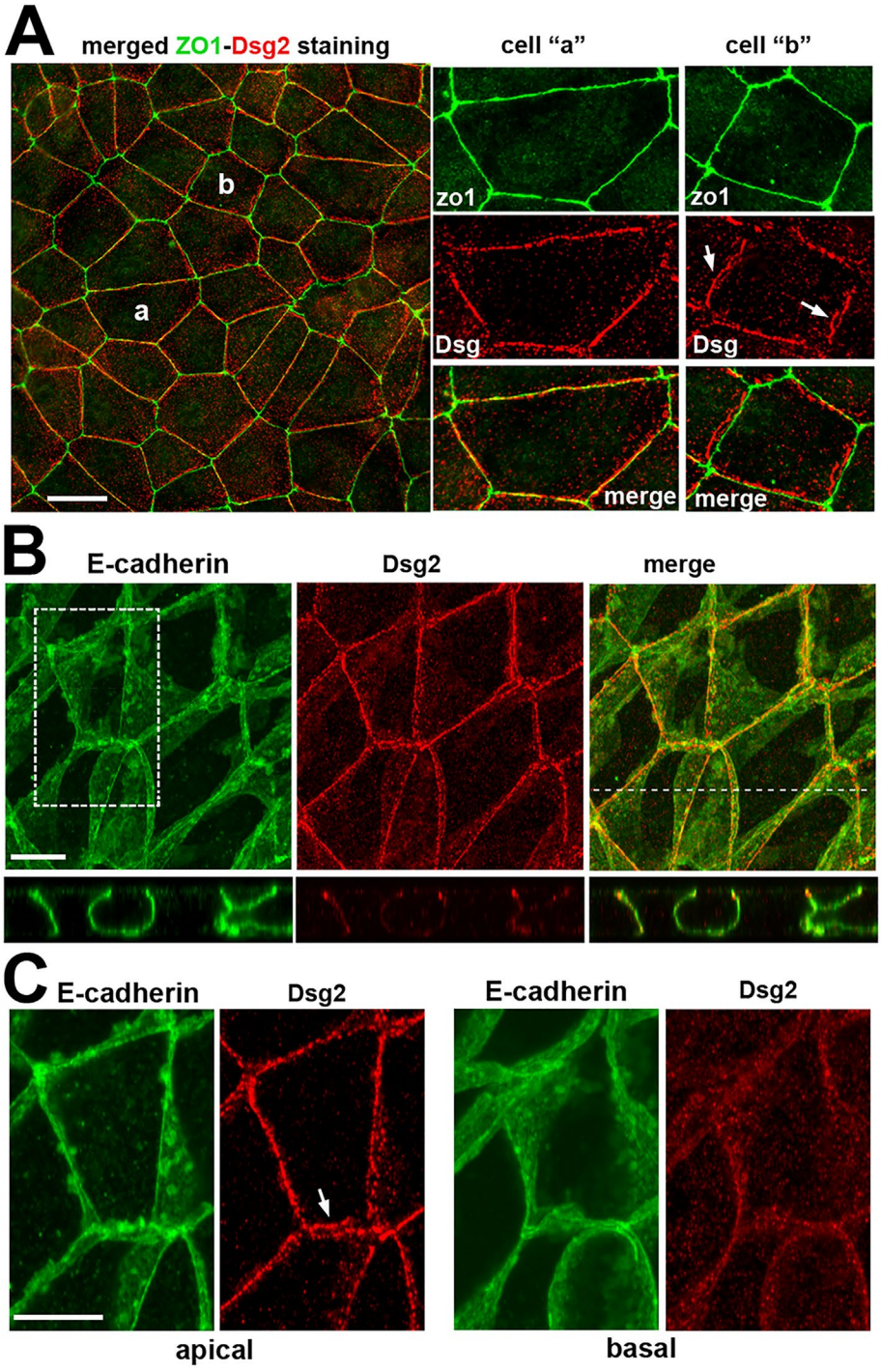

FIGURE 1: Overall distribution of DSMs in DLD1 cells. (A) Representative widefield images of DLD1 in cell culture showing ZO1-stained TJs (green) and Dsg2-stained DSMs (red). Higher magnification of two cells, marked "a" and "b," are shown in the right panels. Note that in a majority of the cells shown here, DSMs are arranged into linear arrays that tightly align with TJs (cell "a"). In some cases, as in the cell "b," the DSM array deviates from TJs. Bars, 20 μm. (B) Confocal images of DLD1 cells stained for the AJ marker E-cadherin (E-cadherin, green) and Dsg2 (red). Projections of all x-y optical slices are shown. Bar, 10 μm. The optical z–cross-sections along the white line of the merged image are shown at the bottom. Note that the linear arrays of DSMs are aligned with AJs. (C) The zoomed area indicated by the dashed box in B. Projections of optical z slices spanning apical (apical) and basal (basal) portions of the cells are presented. The apical region is reconstructed by a projection of three optical z slices spanning the most apical 1.5 μm of the cells. The basal region is a projection of all nine remaining optical z slices spanning 4.5 μm of the cell positioned between the apical region and the basal cell membrane. Note that even those DSM arrays that deviate from the AJC (arrow) are located within the apical section of the cells. Apicobasal distribution of desmosomes is quantified in Figure 3, C and D. Bar, 10 μm.

In Pkp3-KO cells the number of rDSMs was dramatically decreased and the remaining sparse rDSMs did not form clear AJC-associated arrays. Instead, the rDSMs were irregularly positioned along the lateral membrane (Figure 3, A and B, quantified in Figure 3, C and D). Overall, our genetic analysis raises the possibility that Pkp3 is involved in integrating DSMs into the AJC. A significant increase in the abundance of basal DSMs in Pkp2-KO cells suggests that Pkp2 may play a cooperative role in spatial DSM organization. It is also important to note that E-cadherin staining was not detectably changed in these cells, showing that apically located zonula adherens and numerous so-called spotlike AJs were still abundant along the lateral membrane.

Joint function of Pkp2 and Pkp3 is essential for DSM assembly

If Pkp2 and Pkp3 play complementary roles in mechanisms leading to the association of DSMs with AJC, their joint inactivation should completely abolish this process. Indeed, it has been shown that simultaneous silencing of Pkp2 and Pkp3 completely disrupts DSM assembly (Todorovic *et al.*, 2014; Fujiwara *et al.*, 2015). To verify that DLD1 cells are not an exception, we generated DLD1 cells in which both Pkp2 and Pkp3 were knocked out (Figures 2 and 4, Pkp2/3-KO). These cells showed no significant changes in their general morphology or organization of their cell–cell contacts, as could be judged by E-cadherin or ZO1 distribution (Figure 4). Further, no changes were detected in the expression of other tested DSM proteins (Figure 2B). However, in agreement with previous observations, these cells were unable to form DSMs. Instead, Dsg2 in these cells was broadly distributed along both the basolateral and the apical membranes of the cells (Figure 4). The surface localization of Dsg2 in these cells was further validated by staining nonpermeabilized cells with an antibody specific for the extracellular Dsg2 region (Supplemental Figure S2). This result shows that a joint function of Pkp2 and Pkp3 is essential for DSM assembly. Furthermore, the observation that Dsg2 is still delivered to the surface and no longer restricted to the lateral membrane, despite apparently

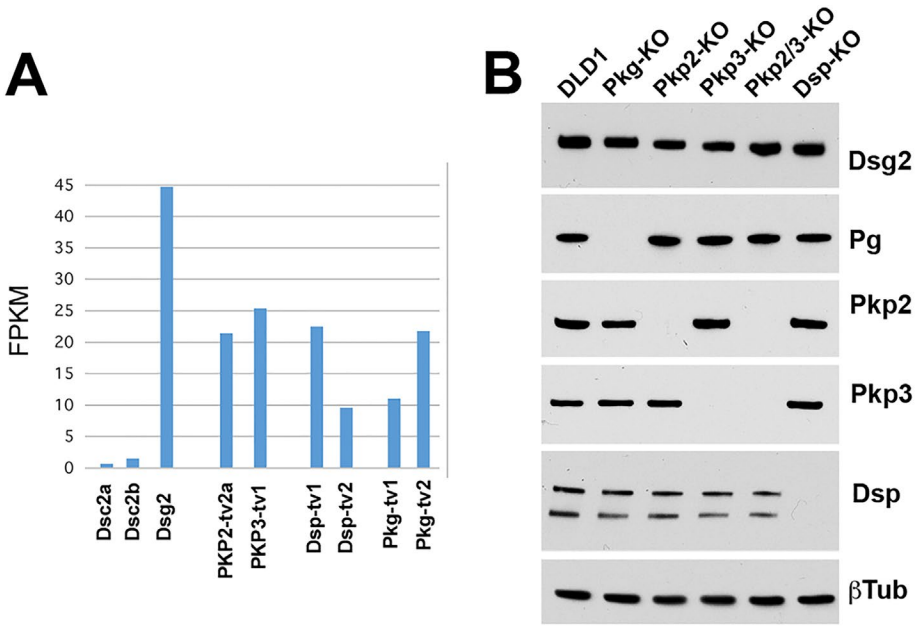

FIGURE 2: Expression profile of DSM proteins in DLD1 cells and their KO progenitors. (A) FPKM for each of DSM protein genes obtained from the RNA-seq analyses of DLD1 cells. (B) Western blot characterization of the major DSM proteins expressed in wt DLD1 cells and in their progenitors obtained after KO of specific DSM proteins, Pg-KO, Pkp2-KO, Pkp3-KO, Pkp2/3-KO, and Dsp-KO. The presented Western blots were obtained from the same experiment using the same set of protein samples for each blot. β-Tubulin staining (βTub) serves as a loading control. Data are representative of three independent experiments. Note that the lack of any of the major DSM proteins does not significantly change the expression levels of other tested proteins.

unperturbed formation of AJs, suggests that interactions mediated by the Dsg2 ectodomain, including its adhesive interactions (Harrison *et al.*, 2016) and its *cis* interactions with E-cadherin (Shafraz *et al.*, 2018), are too weak to entrap this protein in cell–cell contacts.

Pkp3 is localized at cell–cell contacts in two distinct, DSM-associated and extraDSM pools

Since Pkp3 KO led to the most severe abnormalities in apicobasal distribution of DSMs, we next analyzed whether Pkp3 itself exhibited any kind of apicobasal polarity (ABP) in wt DLD1 cells. In agreement with previous studies, immunofluorescence microscopy showed that Pkp3 was a constituent of nearly all DSMs, which were identified using Dsg2 (Figure 5A) or Dsp (Supplemental Figure S1) antibodies. However, Pkp3 also resided in additional locations. In fact, the brightest Pkp3 staining was associated not with DSMs but with cell vertices, also known as tC contacts, where the corners of three or more cells meet. These Pkp3-enriched contacts often exhibited no detectable Dsg2 or Dsp fluorescence (arrowheads in Figure 5B and Supplemental Figure S1). Furthermore, Pkp3 localization was not restricted to DSMs along the bicellular (bC) contacts: Pkp3 was also evident between and around DSMs (arrows in Figure 5B). Interestingly, a significant pool of Pkp3 in both tC and bC contacts was often more apical than DSMs, as clearly seen in optical sections (Figure 5, A and B) or in the Z-plane view of a selected cell–cell contact (Figure 5C).

We further assessed the size of the extraDSM Pkp3 pool by calculating the Pearson's correlation coefficient (PCC) between Dsp or Dsg2, which marked DSMs, and Pkp3. The average Pearson's values (~0.6–0.7 for both Dsp-Pkp3 and Dsg2-Pkp3) were significantly higher than those obtained for only tC areas (0.2 and 0.4, correspondingly), which were manually demarcated as a circular, 5 μm in diameter, areas around each of tC contacts present in the same images (Figure 5D). The centers of the "tC circles" were positioned at the intersections of the three or more cell borders. The greatest overlap (~0.7) between Dsp (or Dsg2) and Pkp3 was detected in the bC areas.

To specify the localization of Pkp3 in tC contacts, we analyzed the relative distribution of Pkp3 with tC TJs and AJs (tC-TJs and tC-AJs). Interestingly, neither of these two junction types completely matched the tC pool of Pkp3. However, staining for the tC-TJ marker MARVELD-2 (known also as tricellulin) showed that tC-TJs were typically located at the core of the Pkp3 tC pool, while the sites enriched with vinculin, the marker of tC-AJs, were often at the periphery of this pool (Figure 5E). As expected, a PCC determined for Pkp3 and MARVELD-2 fluorescence in the tC area was significantly higher than that for Dsp and MARVELD-2 (Figure 5D).

Taken together, the immunolocalization data strongly suggest that the extraDSM pool of Pkp3 at least partially associates with both tC-TJs and tC-AJs. To validate this point, we used an in situ proximity ligation assay (PLA). The PLA fluorescent signal is generated by the rolling cycle amplification reaction between a pair of oligonucleotide-labeled secondary antibodies. The reaction efficiently proceeds only when two probed antigens are < 40 nm of each other. Here we used three different rabbit antibodies, directed against Dsg2, ZO1, and β-catenin, combined with the same mouse anti-Pkp3 antibody. After performing the amplification reaction, the rabbit antibody was additionally stained by anti-rabbit IgG to allow us to assign the PLA signal to specific junctions. As a negative control, DLD-Pkp3-KO cells were used. The PLA detected Pkp3 in proximity to all three major AJC junctions (Figure 5, F and G). As expected, of these three, the Dsg-Pkp3 probe produced the brightest signal. However, the majority of signals generated by ZO1-Pkp3 resided along the cell–cell contacts, while Dsg2-Pkp3 signals were more broadly distributed. Quantification of the tC/outside tC PLA index, determined as a ratio of the PLA signal detected within 5 μm tC circles centered at tC junctions (positioned as indicated above) to the total signal outside of these circles, showed that ZO1-Pkp3 and β-catenin-Pkp3 pairing was 10 and 3 times more specific to tC junctions than that of Dsg2-Pkp3 (Figure 5G).

Pkp2 and Pkp3 position in DLD1 cells is controlled independently

It was reported that Pkp3-enriched DSMs are concentrated within tC-DSMs in keratinocytes, and that Pkp1 KO results in redistribution of Pkp3 away from tC contacts toward bC-DSMs (Keil *et al.*, 2016). In contrast to keratinocytes, our results show that in DLD1 cells Pkp3 is not only enriched in DSMs but also abundant in the extraDSM pool, which is especially pronounced in tC contacts. To address whether Pkp2 and Pkp3 localization and/or functions are interdependent in DLD1 cells, we first stained wt DLD1 cells for Pkp2.

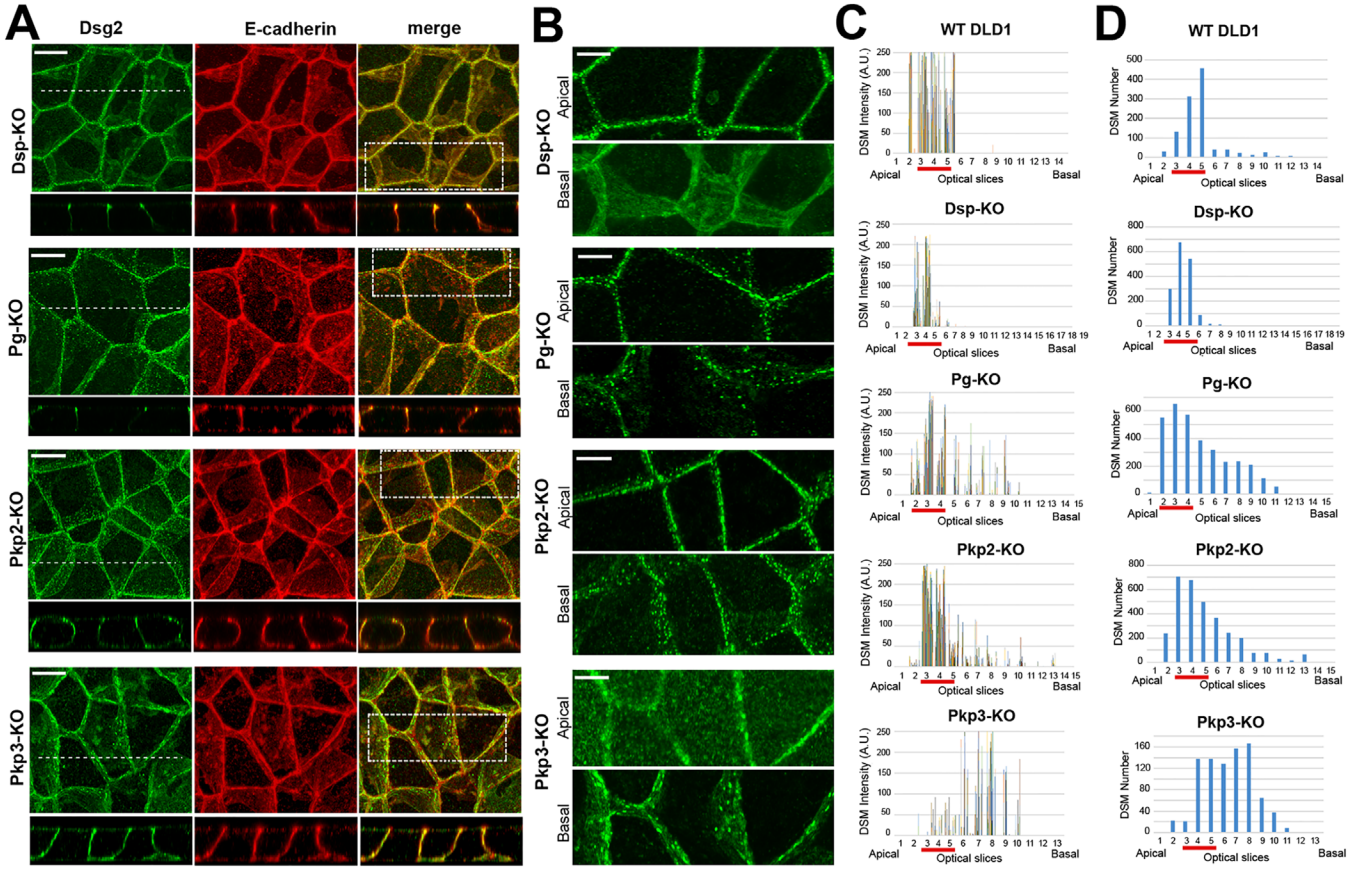

FIGURE 3: Spatial organization of DSMs in cells on KO of major DSM proteins. (A) DLD1 cells deficient for each of four major DSM proteins (Dsp-KO, Pg-KO, Pkp2-KO, and Pkp3-KO) were stained for Dsg2 (green) and E-cadherin (red) as shown for wt DLD1 cells in Figure 1B. Projections of all x-y optical slices are shown. Bar, 10 μm. The optical z–cross-sections along the white dashed lines (depicted in Dsg2 images) are shown at the bottom. (B) The cell areas indicated by dashed boxes in A were split into two "apical" and "basal" halves as in Figure 1C for wt DLD1 cells. Note that DSMs are significantly more abundant in the apical region in Dsp-KO, Pg-KO, and Pkp2-KO cells. This situation is reversed in the Pkp3-KO cells. Note that the heights of the cells slightly vary from sample to sample, resulting in different numbers of confocal slices. Bar, 5 μm. (C) Apicobasal plots of DSM fluorescence intensity (bars of different colors represent individual DSMs) and (D) their abundance along the confocal slices (the step is 0.5 μm). The graphs quantify the full-view images (50 × 50 μm^2) presented in A and the control WT DLD1 cells presented in Figure 1B. Note that each image contains about eight cells. The slice numbering starts from the slice in which the most apical features in at least one cell are in focus. The slices presenting AJC are highlighted with a red line. The slightly different number of slices is due to some variability in the cell heights. A.U., arbitrary unit. Data are representative of three independent experiments.

Immunofluorescence microscopy showed that in formaldehyde-fixed cells, Pkp2 localization in both DSMs and tC contacts was significantly weaker than Pkp3 (Figure 6A, some of Pkp2-enriched tCs are indicated by arrows). This weak Pkp2 staining was specific since it was completely undetectable in Pkp2-KO cells (Figure 6B). It is likely that weak Pkp2 staining was caused by epitope masking since it was dramatically increased using an alternative fixation protocol (see Supplemental Figure S2C). No obvious differences in Pkp2 distribution were detected in Pkp3-KO cells by visual inspection of the samples (Figure 6C).

We then tested whether KO of Pkp2, similar to KO of Pkp1 in keratinocytes, depleted the tC pool of Pkp3. Immunolocalization of Pkp3 in PKP2-KO cells showed that the lack of Pkp2 did not abolish Pkp3 enrichment at tC contacts (Figure 6, D and E). Thus, localization of Pkp2 and Pkp3 in DLD1 cells is controlled in a largely independent manner. Nevertheless, their shared localization at tC contacts and the cumulative effect of their loss on DSM assembly suggest that they can cooperate functionally (see above).

Polarity proteins from Scrib module play a minor role in Pkp3 localization

The results described above indicate that Pkp3 KO disturbs integration of DSMs into the AJC (Figure 3) and that a significant fraction of Pkp3, especially pronounced in tC contacts, resides outside of DSMs. This extraDSM fraction overlaps with tC-TJs and/or tC-AJs. These observations suggested that Pkp3 might link DSM assembly with ABP mechanisms, which guide the localization of AJs and TJs (Dow and Humbert, 2007; Tepass *et al.*, 2001). Little is known about the role of ABP polarity proteins in global organization of DSMs. First we validated that the presence of extraDSM pool is not a specific feature of DLD1 cells, but also is prominent in three other polarized epithelial cell lines: immortalized epithelial kidney cells, MDCK, human bronchial epithelial cells, HBE, and another colon carcinoma cell line, Caco2 (Supplemental Figure S3A). We then tested whether the overall distribution of DSMs and/or Pkp3 localization in tC contacts depended on the core ABP signaling proteins. To this end, two types of DLD1 cell mutants, characterized in our recent paper

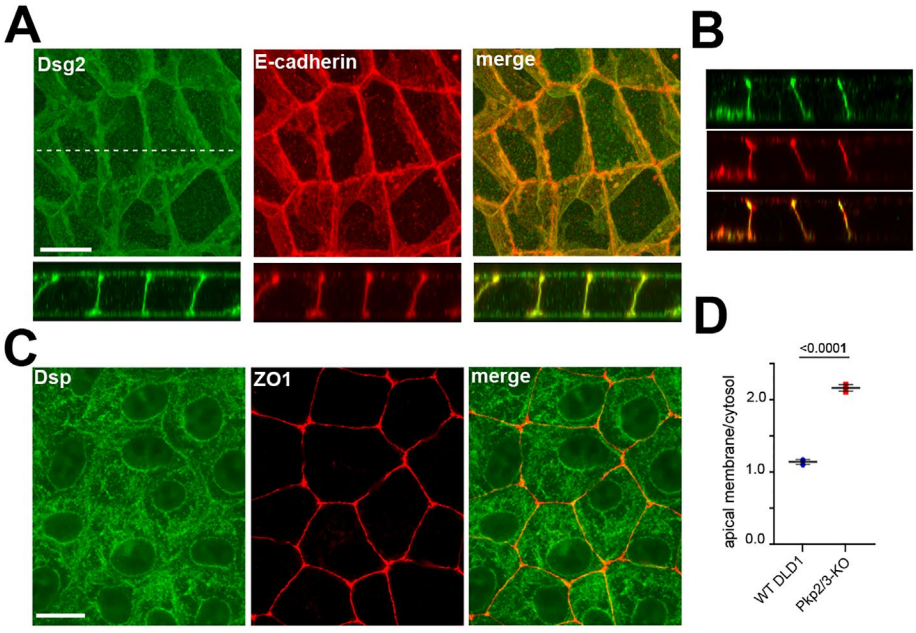

FIGURE 4: Dsg2 and Dsp in DLD-Pkp2/3-KO cells. (A) The Pkp2/3-KO cells were stained for Dsg2 (green) and E-cadherin (red) and imaged by confocal microscopy. Projections of all x-y optical slices are shown. Bar, 10 μm. The optical z–cross-sections along the white dashed line (depicted in the Dsg2 image) are shown at the bottom. (B) Representative widefield image of DLD1 cell culture showing ZO1-stained TJs (red) and Dsp-stained DSMs (green). Bar, 10 μm. (C) Representative optical z–cross-sections of wt DLD cells stained as in A are shown for comparison. (D) The ratios of the apical to cytosolic Dsg2 fluorescence in WT and Pkp2/3-KO DLD1 cells. The measured apical areas do not include cell–cell contacts. Black bar shows *t* test *p* values.

(Choi *et al.*, 2019), were evaluated for DSM and Pkp3 subcellular distribution.

We first tested Llgl1/2-deficient DLD1 cells. We previously showed that the apical identity Par complex (determined by Par6-aPKC) is depolarized in these cells and expanded from the apical into the lateral membrane. Despite these polarity defects, Llgl1/2-KO cells show no significant disorganization of TJs or AJs (Choi *et al.*, 2019). Here, staining for DSM markers showed that the apically located DSM arrays were largely preserved in these cells (Figure 7A). The apicobasal analyses of DSM distribution confirmed a predominant localization of DSM in the apically located slices of the confocal z-stacks (Figure 7E). The Lgl1/2-KO cells also exhibited a pronounced extraDSM pool of Pkp3 in tC contacts, which was even more prominent than that in the wt DLD cells (Figure 7A and arrowhead in Figure 7B). In agreement with this observation, the average Dsp-Pkp3 Pearson's correlation in tC contacts of these cells (Figure 7F) was significantly lower (just 0.12) than that in the wt cells (0. 22). Furthermore, the bC contacts of these cells, while still exhibiting a high Dsp-Pkp3 correlation (~0.65), also clearly displayed a DSM-free pool of Pkp3 (see arrows in Figure 7B). Double staining for Pkp3 and TJ markers ZO1 and MARVELD-2 demonstrated that this extraDSM Pkp3 pool was in proximity to TJs (Figure 7, A and B).

We next tested DLD20-2 cells, deficient for three LAP proteins, Scrib, Erbin, and LANO. We previous reported that in these cells both Par6-aPKC and Crumbs (detected by the protein PALS) complexes are depolarized. We previously showed that these cells exhibit a dramatic depolarization of the AJC, with pronounced fragmentation of TJs and expansion of the TJ fragments from the apical to more basal regions of the lateral membrane (Choi *et al.*, 2019). Here, immunofluorescence analysis showed that DSMs in these cells also lost apical localization and could be observed in the middle section of their lateral membranes (Figure 7C, see optical cross-sections, and Figure 7E). However, while misplaced, the majority of DSMs were still organized in linear arrays along TJs, clearly detectable using both anti-Dsp (Figure 7C) or anti-Dsg2 (Supplemental Figure S3B) antibodies. The extraDSM pool of Pkp3 was pronounced in tC contact areas of these cells and co-localized with MARVELD-2 (Figure 7, C and D). Furthermore, this extraDSM pool was often notable in bC areas (arrow in Figure 7D, and Supplemental Figure S3B). In line with the general disorganization of TJs, the positions of tC junctions in DLD20-2 cells did not always coincide with the geometrical intersections of cell borders. Therefore, to compare the Pearson's correlation between tC and bC contacts in DLD20-2 cells, 5 μm-wide tC circles were positioned based on MARVELD-2 localization using triple-stained (Dsp/Pkp3/MARVELD-2) samples. This assessment indicated that DLD20-2 cells have the lowest correlation value, just 0.08, between Dsp and Pkp3 in tC contacts (Figure 7F).

Collectively, these data confirm that loss of function of the Scrib polarity module results in general disorganization of the AJC without disrupting association of DSM arrays with TJs or overall integrity of the tC-TJs, suggesting that the mechanisms responsible for coordinated assembly of AJC components are largely preserved in these cells. Further, the extraDSM pool of Pkp3 still localized, and was even enhanced, in tC compared with wt cells. The latter observation is consistent with the possibility that the extraDSM pool of Pkp3 is under negative control of Scrib module proteins.

Organization of the extraDSM pool of Pkp3 is controlled by the apical identity protein Par3

TJs demarcate the border between apical and basolateral regions of the cell and also provide a scaffold for localization and function of one of the key apical polarity proteins, Par3. Proximity of Pkp3 to ZO1, which is indicated by a strong ZO1-Pkp3 PLA signal, suggested that Pkp3 could directly encounter Par3. To address this possibility, we carried out PLA analysis for Pkp3 and Par3. As predicted, the Par3-Pkp3 antibody pairing resulted in a high PLA signal in wt cells, but not in Pkp3-KO cells (Supplemental Figure S4, A and B). These data prompted us to test the contribution of Par3 to DSM organization. To this end, the major Par3 parolog, PARD3A, was knocked out by oligonucleotide targeting all 6 PARD3A variants identified in DLD cells by RNA-seq (see Supplemental Figure S4C, D). Using these cells as a negative control in Par3-Pkp3, PLA experiments demonstrated that the PLA signal for this antibody pair is specific (Supplemental Figure S4). Importantly, in agreement with published data (Joberty *et al.*, 2000; Hirose *et al.*, 2002; Chen and Macara, 2005), the resulting Par3-KO cells showed gross abnormalities in general organization characterized by fragmentation of TJs (Figure 8) and disintegration of the beltlike apical AJs. AJs were retained at the lateral cell membranes, however (Supplemental Figure S4). Staining for the set of apical and basolateral polarity proteins

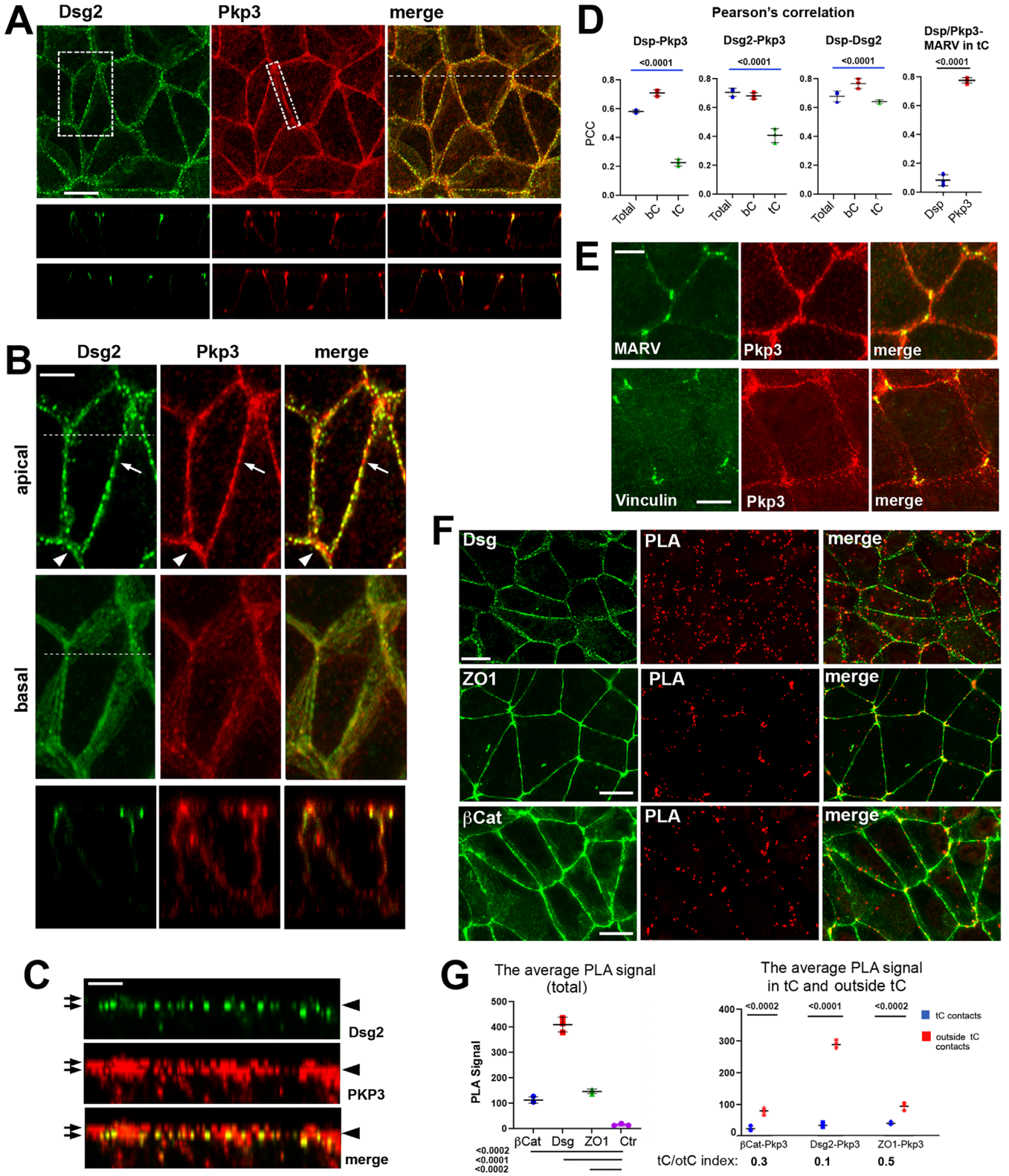

FIGURE 5: Dual localization of Pkp3 and other junctional proteins in DLD1 cells. (A) Wt DLD1 cells were stained for Dsg2 (green) and E-cadherin (red). Projections of all x-y optical slices are shown. Bar, 10 μm. The optical z–cross-sections along the white dashed lines (depicted in Dsg2 image) are shown at the bottom. (B) The cell areas indicated by dashed boxes in A were split into two "apical" and "basal" halves as described in Figure 1C. Note that the majority of Pkp3 is localized in the apical cell portion together with Dsg2-enriched puncta. However, Pkp3 was also located outside of desmosomal puncta in both bC contacts (arrow) and tC contacts (arrowhead). The optical z–cross-sections show that a proportion of Pkp3 is more apical than DSMs. Bar, 5 μm (C) A Z-plane slice of the cell–cell contact marked by dashed line in A. Bar, 3 μm. Note that the majority of DSMs are located within a single confocal frame (arrowhead), while Pkp3 is

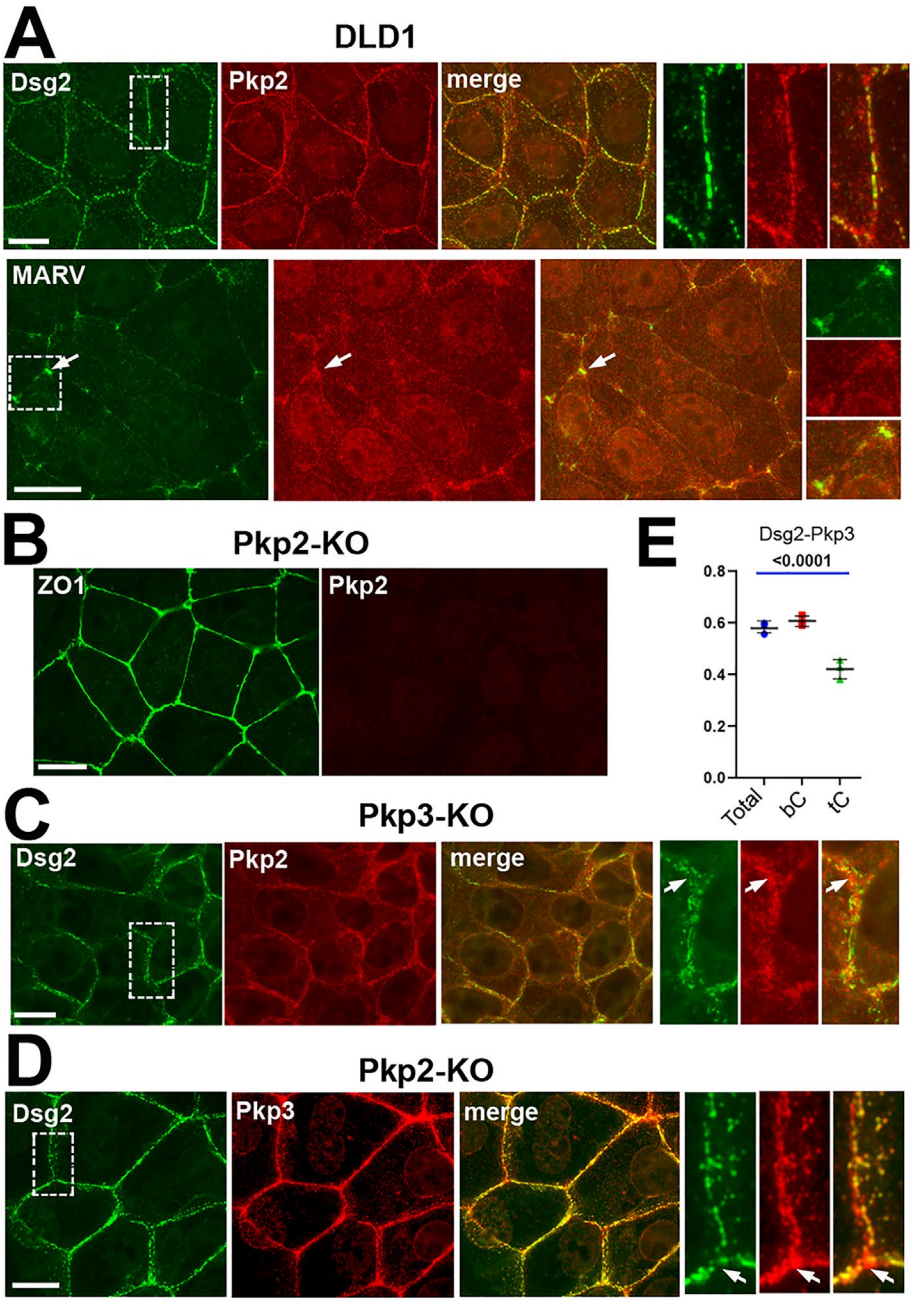

confirmed that the apical domain of these cells was severely affected and acquired traits of the basolateral membrane. Indeed, the apical identity polarity protein, PALS, which is located at the apical membrane in control cells, became cytosolic and was replaced with basolateral Scrib module proteins, Llgl1/2 and Scrib (Supplemental Figure S4, E ands F).

Staining these cells for DSM markers revealed a remarkable disorganization of DSMs. A distinguishing feature of the Par3-KO cells was that a significant fraction of Dsg2 was broadly dispersed along the apical

FIGURE 6: Pkp2 and Pkp3 localizations are mutually independent. Representative widefield images of corresponding cell cultures are shown. The tC contact areas indicated by dashed boxes are zoomed in the right panels. Bars, 10 μm. (A) Wt DLD1 cells are co-stained for Pkp2 (red) and either for Dsg2 (Dsg2) or tC-TJs marker MARVELD-2 (MARV). Note that Pkp2 in tC contacts (arrows), similar to Pkp3, is localized outside of Dsg2-marked DSMs and roughly overlaps with tC-TJs marked by MARVELD-2. (B) Double staining for Pkp2 (Pkp2, red) and ZO1 (ZO1, green) in Pkp2-KO cells. A complete absence of Pkp2 staining in these cells demonstrates specificity of Pkp2 staining in the control wt DLD1 cells presented in A. (C) Dsg2-sPkp2 staining in Pkp3-KO cells. Note that the lack of Pkp3 did not abolish foci of Pkp2 staining at tC contacts (one example is indicated by an arrow in the zoomed area). (D) DLD-Pkp2-KO cells were co-stained for Pkp3 (Pkp3, red) and Dsg2 (Dsg2, green). Note that Pkp3 in these cells is still enriched in the tC areas (arrows). (E) PCC for Dsg2-Pkp3 pair taken from randomly selected images (Total), only for bC contacts (bC), or only for tC contacts (tC). The blue bar represents one-way ANOVA *p* value.

also abundant in one additional apical frame (arrows). (D) PCC for Dsp-Pkp3, Dsg2-Pkp3, Dsp-Dsg2 pairs quantified for full-view images (Total), only for bC contacts (bC), or only for tC contacts (tC). PCC for Dsp-MARVELD-2 (MARV) and for Pkp3-MARVELD2 was taken only for tC contacts. For quantification details, see *Materials and Methods*. Blue and black bars represent one-way ANOVA or *t* test *p* values, correspondingly. (E) DLD1 cells were double stained for Pkp3 (red) and for markers of tC-TJs, MARVELD-2 (MARVELD-2, green) or tC-AJs, vinculin (vinculin). Note that MARVELD-2 is typically located at the center, while vinculin could be seen at the periphery of the Pkp3 tC-enriched zone. Bars, 5 μm (F) PLA with DLD1 cells using rabbit Dsg2 (Dsg), ZO1 (ZO1), β-catenin (βCat) antibodies, and mouse anti-Pkp3 antibody. Rabbit antibodies were visualized by anti-rabbit IgG (green). Note that the ZO1-Pkp3 PLA signal is enhanced in tC contacts. (G) The PLA signal was quantified in two different ways. Left diagram (The average PLA signal, total) shows the average PLA signal per image in a confluent culture (90 μm × 67 μm). In the right diagram (The average PLA signal in tC and outside tC), the PLA signal was split between tC contacts (determined as a 5-μm circle around a point of tC contacts) and the remaining area in each image. Black bars represent *t* test *p* values.

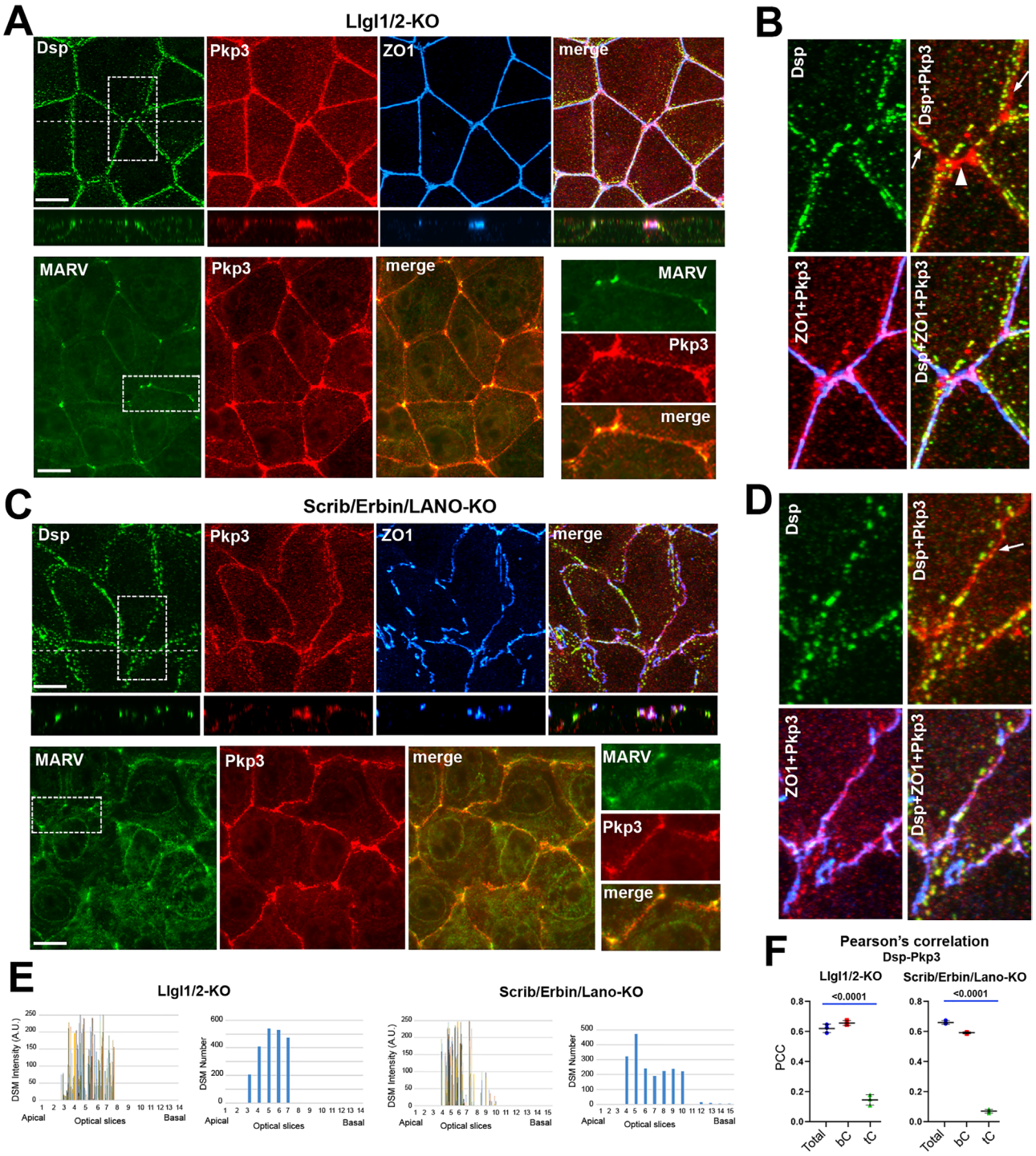

FIGURE 7: Basolateral identity proteins from the Scrib module are not essential for tC localization of Pkp3 and localization of DSMs in the AJC. (A) Llgl-deficient DLD1 cells (Llgl1/2-KO) were triple stained for Dsp, Pkp3, and ZO1, or double stained for MARVELD-2 (MARV) and Pkp3 and imaged in the confocal (in the first) or widefield (in the second case) microscopy. Note that Pkp3 is enriched in tC junctions and DSMs are organized into apical arrays as it is the case for wt DLD1 cells. Bars, 10 μm. (B) The localization of Desmoplakin (Dsp), Dsp and Pkp3 (Dsp+Pkp3), ZO1 and Pkp3 (ZO1+Pkp3), and all three markers together (Dsp+ZO1+Pkp3) for cell area are indicated by dashed boxes in the triple-stained image in A. Note that different pools of Pkp3 are co-localized with both DSMs and TJs. (C) LAP protein-deficient DLD20-2 cells (Scrib/Erbin/LANO-KO) were stained as indicated in A. Note that despite the significant disorganization of the cells, DSMs still align with TJs and PKP3 is enriched in tC contacts, where it partially overlaps with MARVELD-2. (D) The zoomed area indicated by the dashed box in (C) is presented in four staining combinations as indicated in B. (E) The apicobasal plots of DSM distribution and their abundance derived from the full-view confocal images presented in A and in (C). See Figure 3 for details. (F) PCC for Dsp-Pkp3 taken for the entire images (total), only for bC contacts (bC), or only for tC contacts (tC). In the case of Scrib/Erbin/Lano-KO cells, the tC contacts were selected based on MARVELD-2 staining. The blue bar represents one-way ANOVA *p* value.

and lateral cell membranes (Figure 8A). This abnormal localization, which was not observed in Scrib module-deficient cells (see Supplemental Figure S2), made it difficult to define individual DSMs based on Dsg2 staining. However, using staining for Dsp, numerous DSM-like puncta were detectable (Figure 8, B and C). Plotting the Dsp puncta along the optical z-slices revealed that they lost the preferred localization at the cell apex and were also abundant in the middle sections of the lateral membrane (Figure 8E). It should also be noted that in these cells a strong Dsp and Dsg2 signal derived not only from lateral but also the apical surface of these cells (arrows in Figure 8A). These apical Dsp puncta in Par3-KO cells may represent nonadhesive cis-clusters of DSM proteins or abnormal DSMs formed between juxtaposed folds of the same membrane.

Despite such abnormalities, the Dsp-containing DSM puncta in the Par3-KO cells clearly incorporated Pkp3 (Figure 8, B and C) with an average Pearson Dsp-Pkp3 correlation value of 0.6, the same as in wt DLD cells (Figure 8F). A striking feature of Par3-KO cells that distinguishes them from cells defective for Scrib polarity module was a complete absence of tC-TJs defined by MARVELD-2 staining (Figure 8D). The extraDSM pool of Pkp3 was also undetectable, consistent with a role for Par3 in maintaining this pool (Figure 8, B and C). Consistently, Pearson's Pkp3-Dsp correlation for tC contacts (defined by geometrical criteria since MARVELD-2 was absent) showed no difference from that of the bC contacts (Figure 8F). Altogether, our data showed that Par3 deficiency led to significantly more dramatic DSM and Pkp3 abnormalities than Scrib module deficiency.

Finally, to validate that the observed DSM phenotype in Par3-KO cells was specific, we expressed GFP-tagged Par3 in the Par3-KO cells. The resulting stably transfected cell line exhibited a complete restoration of TJs (Figure 8H and Supplemental Figure S4D). Correspondingly, the DSMs in these cells became detectable by Dsg2 staining (Supplemental Figure S4G) and showed a clear preference for the apical portions of the lateral membranes (Figure 8E). Furthermore, reintroduction of Par-3 also rescued the tC contact-located extraDSM pool of Pkp3 as observed by visual inspection (Figure 8G) as well as by differences in Pearson's Pkp3-Dsp correlation between tC and bC contacts (Figure 8F).

DISCUSSION

Desmosomes are evolutionarily recent innovations, having joined AJs and TJs as part of the polarized AJC in simple epithelia of vertebrates (Rübsam *et al*., 2018). While mechanisms dictating the polarized distribution of AJs and TJs in the apical region of the basolateral membrane have been uncovered, how DSMs might be integrated with this network was unknown. The role of Dsp in this process has been suggested by recent BioID proximity proteomics that shows a juxtapositioning of this DSM protein with some polarity proteins, such as Par3 or Scribble (Badu-Nkansah and Lechler, 2020). The work described here suggests that interplay between another DSM protein, Pkp3, and that apical polarity protein, Par3, could play a fundamental function in coordinating DSM assembly into, and maintenance in, the AJC proper.

It has been shown that TJs and AJs are localized at the apical end of the lateral membrane in DLD1 cells, making these cells suitable to study ABP (Abe and Takeichi, 2008; Choi *et al*., 2019). Here we show that DSMs, the third component of AJC, are assembled along TJs and AJs within the AJC of DLD1 cells. Consistent with previous genetic data, the individual inactivation of any major DSM protein in DLD1 cells does not abolish DSM assembly. However, KO of Pkp3, while not disturbing TJs and AJs, uncouples DSMs from the AJC, leading to spreading of DSM complexes all along the basolateral membrane domain. Genetic ablation of other DSM molecules did not interfere with DSM's association with the AJC. This observation establishes Pkp3 as unique among the DSM molecules tested in functionally linking DSMs with the polarized AJC.

Although loss of Pkp2 did not uncouple DSMs from the AJC, the joint inactivation of both Pkp2 and Pkp3 completely abolished DSM assembly, including the formation of rDSMs marked by Dsg2 clusters. This observation is in line with previous work showing that cooperation among Pkps is essential for DSM formation (Todorovic *et al*., 2014; Fujiwara *et al*., 2015) and desmosomal cadherin clustering (Fujiwara *et al*. 2015). A critical role of Pkps in Dsg clustering is also supported by the Pkp2-induced clustering of Dsg2 in Pkp-deficient HT1080 cells (Koeser *et al*., 2003) and Pkp1-dependent clustering of Dsg as demonstrated by cross-linking analyses (Fuchs *et al*., 2019). Taken together with our biochemical data showing a remarkably broad binding capacity of Pkps (Chen *et al*., 2002; Bonné *et al*., 2003;), the available data suggest that Pkps provide an essential "structural framework" for Dsg and Dsc clusters. Furthermore, the observation that DSMs fail to become polarized in Pkp3-KO cells suggests that Pkp2, while partially compensating for Pkp3 in DSM assembly, cannot build such a "framework" in conjunction with the polarity machinery.

Immunostaining for Pkp3 shows that its localization is not restricted to DSMs. Inspection of confocal stacks, Pearson's Pkp3-Dsg2/Dsp correlations, and PLAs indicate that an extraDSM pool of Pkp3 is closely associated with TJs and/or AJs in the AJC. This pool is especially prominent in tC contacts, where it partially overlaps with the specific tC-TJ marker, MARVELD-2. Accordingly, the Pkp3-ZO1 PLA signal is enhanced in tC-contacts, while the Dsg2-Pkp3 PLA signal is not. Future work is required to understand how this extraDSM pool of Pkp3 is formed. It is possible that the cortical localization of extraDSM pool of Pkp3 is partially mediated by direct interactions of Pkp3 with the plasma membrane due to Pkp3 palmitoylation (Roberts *et al*., 2014) and further enhanced by specific protein–protein interactions. Interestingly, in keratinocytes Pkp3 is also targeted to tC contacts, but in this case to tC-DSMs. This tC-DSM targeting of Pkp3 in keratinocytes is suppressed by Pkp1-KO and is facilitated by a specific phosphorylation of Pkp3 (Keil *et al*., 2016; Rietscher *et al*., 2018). While Pkp3 in tC contacts in DLD1 cells resides outside of DSMs and is Pkp1 independent, it is plausible that tC contact enrichment of Pkp3 in keratinocytes and in DLD1 cells could be mechanistically related.

An important question is whether these two Pkp3 pools, one that is required for DSM assembly and another that is found in tC-contacts, are functionally interconnected. Our data support the idea that these two pools are both regulated by the ABP signaling machinery. Consistent with this, DSMs in Pkp3-KO cells are no longer restricted to the AJC, becoming more scattered along the lateral plasma membrane. In addition, the observed ZO1-Pkp3 and Par3-Pkp3 PLA signals suggest that the extraDSM pool of Pkp3 is proximal to TJs, which not only separate apical and basolateral cell domains but also actively participate in ABP signaling. More direct evidence comes from our experiments comparing the response of DSMs to loss of function of apical versus basolateral polarity machinery. Despite prominent changes in overall AJC distribution, DLD1 cells deficient for components of the basolateral polarity Scrib module, either Llgl1 and Llgl2 or the LAP proteins (Scrib, Erbin, and Lano), do not show notable disturbances in the alignment of DSMs and TJs. Furthermore, the extraDSM pool of Pkp3 located in the MARVELD–2-positive tC contacts is preserved and even enhanced if judged by both visual inspection and Pierson's Pkp3-Dsg/Dsp correlation, even though the extraDSM pool also becomes distributed

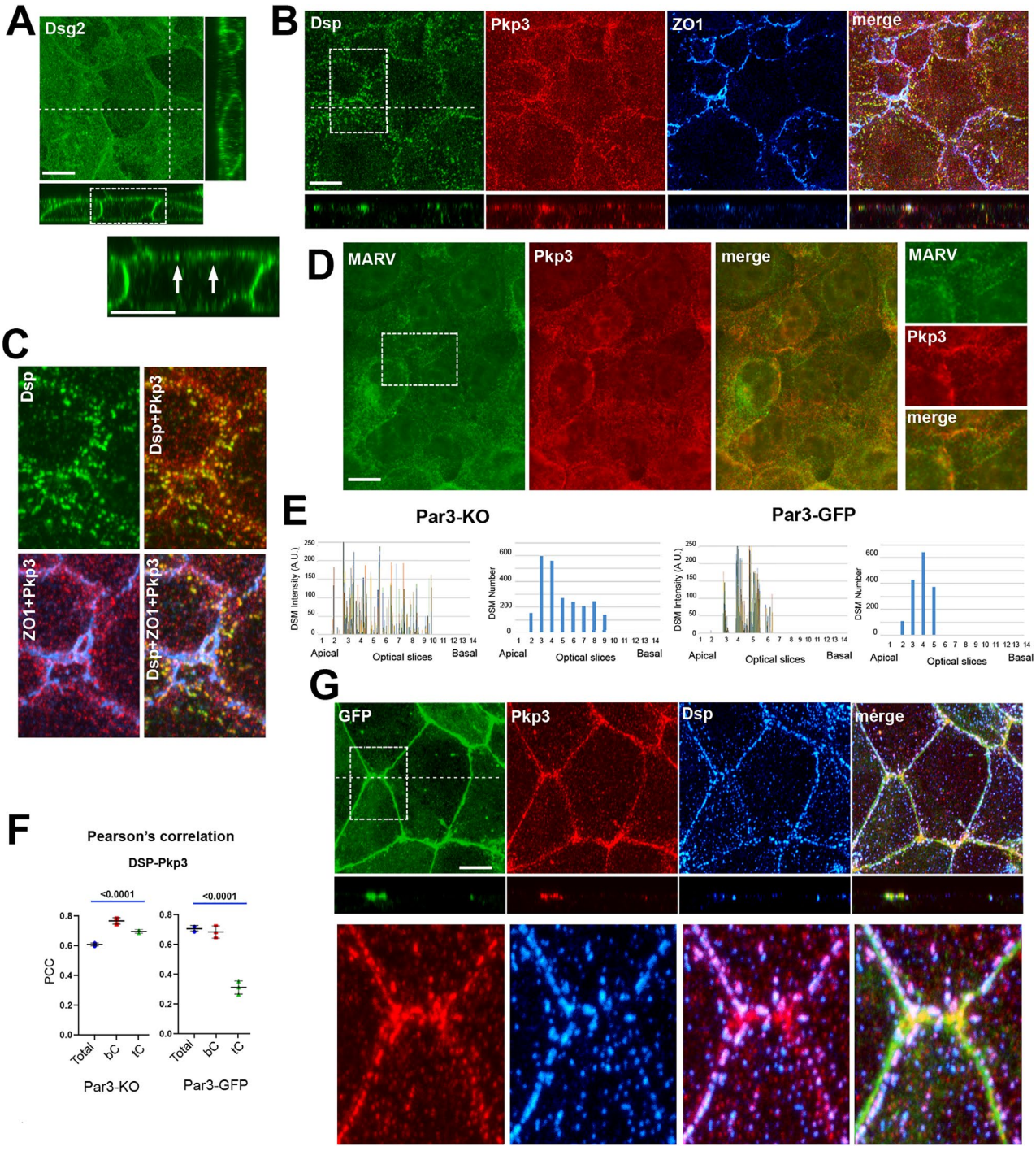

FIGURE 8: Par3-KO cells are unable to correctly organize DSMs and Pkp3. (A) Par3-deficient DLD1 cells were stained for Dsg2 and processed by confocal microscopy. Two optical confocal cross-sections (along the white lines) are presented at the bottom and right margins. The zoomed region of one of the cross-sections is shown below. Note that Dsg2-stained DSMs are hardly visible because of high membranous Dsg2 staining. Also note that Dsg2 also exhibits apical membrane staining. Arrows show two DSM-like puncta on the apical membrane. Bar, 10 μm (B) Confocal image of Par3-KO cells triple stained for Dsp, Pkp3, and ZO1. Bar, 10 μm. (C) The zoomed area indicated by the dashed box in (B) is presented in four staining combinations as indicated in Figure 7B. Note that no extraDSM Pkp3 staining is detectable in tC contacts. (D) The Pkp3 in Par3-KO cells was co-stained with the tC-TJ marker MARVELD-2. Bar, 10 μm. One of the tC contact areas is magnified in the left panel. No MARVELD-2-enriched tC-TJs could be detected in these areas. (E) The apicobasal plots of DSM distribution and abundance derived from the full-view confocal images of Par3-KO cells (Par3-KO) and the same cells after re-expression of GFP-tagged Par3 (Par3-GFP). (F) Pearson's Dsp-Pkp3 correlation coefficient taken for the entire image (Total), only for bC contacts bC), or only for tC contacts (tC, based on geometric criteria). Blue bars represent one-way ANOVA *p* value. (G) The GFP-tagged version of Par3 (Par3-GFP) was reintroduced in the Par3-KO cells and the cells were imaged using confocal microscopy for GFP, Pkp3, and Dsp. Bar 10 μm. The zoomed region indicated by dashed square is shown below.

along the bC contacts. Altogether, these data show that lateral identity proteins control neither Pkp3-dependent integration of DSM into AJC nor the Pkp3 extraDSM pool.

In contrast to the observed preservation of DSM alignment with TJs in cells lacking the basolateral polarity machinery, loss of the apical polarity protein Par3 clearly impaired Pkp3-dependent association of DSMs with AJC and localization of the Pkp3 extraDSM pool. As expected from previous data (Goldstein and Macara, 2007), the apical membrane of Par3-KO DLD cells acquires clear traits of the lateral membrane—the apical PALS protein disappears and is replaced with the lateral identity proteins Llgl1/2 and Scribble. Consequently, these cells, similarly to cells lacking lateral polarity determinants, exhibit disintegration of the honeycomblike pattern of AJC distribution, which becomes fragmented and redistributed along the entire cell–cell contact region. In addition, the DSM phenotype of these two types of cells appeared very different: in contrast to the LAP protein-deficient DLD20-2 cells, Dsg2 in the Par3-KO DLD cells disperses into numerous small clusters, present not only at the lateral cell membranes but also on the apical cell surface. It seems plausible that this phenotype reflects an uncontrolled formation of rDSMs, possibly resulting from deregulation of Pkp3. Another unique feature of the Par3-KO cells is a complete disappearance of the extraDSM pool of Pkp3. Underscoring the relationship between this Pkp3 pool and TJs, MARVELD-2 is also not detectable in the tC-TJ in these cells. Whether such mutual disappearance occurred because one of these structures depends on the other, or they both are independent downstream targets of Par3, is a subject for future research. Since formation of DSMs is reported to depend on AJs, it is important to emphasize that both types of cells (LAP protein deficient and Par3 deficient) formed very prominent E–cadherin-based AJs, whereas the DSM phenotype of these two types of cells appeared very different. Nevertheless, we cannot rule out a possible contribution of local changes in AJs to the observed DSM alterations.

Taken together, our data show that the Par3-KO cells exhibit simultaneous defects in two Pkp3-related processes. First, DSMs are dispersed and lose their alignment with TJs. Second, Pkp3 can no longer be targeted into the DSM-free tC contact-associated pool. While more research is needed to understand whether these two events are functionally interconnected, their parallel occurrence raises the possibility that they are. A possible explanation for such an interrelationship is that Par3 maintains Pkp3 in an "inactive" state, which is unable to interact with DSM targets. In an established polarized epithelial sheet, which we study here, this pool of Pkp3 is concentrated in tC contact areas where no other core DSM proteins are detected. Only a fraction of Pkp3 escapes this Par3-mediated inactivation and functions in DSM assembly. In Par3-KO cells, the majority of Pkp3 is converted to an assembly competent state that is highly active with respect to interactions with DSM proteins (Figure 9). The questions remain: how does Par3 maintain Pkp3 in the tC contact-associated inactive state and how does Pkp3 promote DSM assembly? Based on our understanding of E–cadherin-based adhesion mechanisms (Green *et al.*, 2010; Brasch *et al.*, 2012; Troyanovsky, 2012), it is possible that Pkps produce a cortical protein framework that provides the optimal spacing and stability for cadherin *trans* bonds. And from our work here, specific Par3-dependent modifications may create a Pkp3 pool that is concentrated in tC contacts and unable to assemble into this framework and thus unable to position DSM cadherins in a manner that allows clustering (Figure 9). One of the most attractive modifications that should be tested in future experiments is phosphorylation of Pkp3 by aPKC. This kinase is activated on association with Par3 specifically in TJs (Humbert *et al.*, 2006; Harris, 2017).

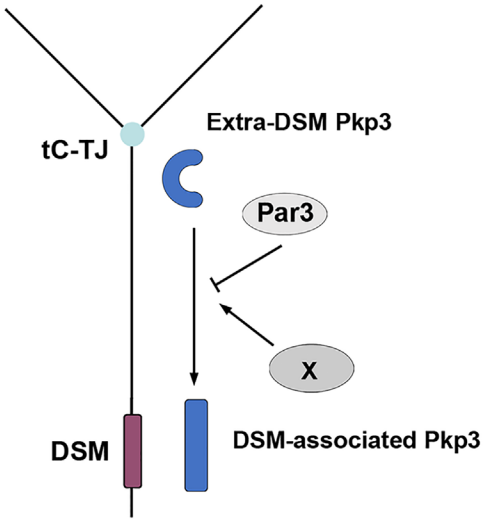

FIGURE 9: Hypothetical model for Pkp3-mediated regulation of DSM assembly. Our data are consistent with the idea that Pkp3 exists in at least two differently located forms. One of these forms (DSM-associated Pkp3) interacts with DSM proteins and is essential component of DSMs (DSM). Another pool of Pkp3 (extraDSM Pkp3) is stored in a vicinity to tC-TJs (tC-TJs). Pkp3 of this pool is unable to associate with DSM proteins. This tC pool, which is "inactive" with respect to DSM assembly, is maintained by a Par3-dependent apical polarity mechanism. Based on this model, a pathway "X" blocks the Par3-dependent negative regulation of Pkp3, which results in conversion of Pkp3 into its DSM assembly-competent form. The active Pkp3 form organizes DSM cadherins into the clusters that are compatible with their adhesive function.

In conclusion, here we take an important step in understanding how cells build their architecture. We pinpoint the signaling process, including a Par3 polarity component, that functions to spatially organize DSMs. Our data also suggest that this process is based on the interplay between two, possibly functionally distinct, pools of Pkp3 that are located in different cell compartments under control of the polarity apparatus.

MATERIALS AND METHODS

Request a protocol through *Bio-protocol*.

Plasmids

pRcCMV-GFP-Par3 was generated using pK-myc-Par3 plasmid (gift from I. Macara, Vanderbilt University, Nashville, TN; 58738; Addgene). The myc portion of this plasmid was replaced with the corresponding one of mGFP (amplified from 21948, pCAG-mGFP-actin; Addgene; a gift from R. Yasuda, Duke University, Durham, NC), and the entire insert of the resulting plasmid was then inserted into the pRcCMV vector (Invitrogen) using *Hin*dIII/*Xba*I sites.

Cell culture and transfection

Transfection and growth of DLD1, MDCK, HBE, and CaCo2 cells and their progenitors were carried out as described (Choi *et al.*, 2019). After antibiotic selection, the cells expressing Par3-GFP were sorted for moderate transgene expression by FACS. The levels and sizes of the recombinant proteins were analyzed by Western blotting. For KO experiments, DLD1 cells stably transfected with the plasmid encoding Flag-tagged Cas9 were used (Choi *et al.*, 2019). Genome editing of these cells was performed using the Alt-R CRISPR-Cas9 System (IDT) also as described (Choi *et al.*, 2019). In

brief, the cells were transfected with an RNA complex consisting of a gene-specific CRISPR RNA (crRNA; designed by software of Broad Institute of Harvard and Massachusetts Institute of Technology) and transactivating RNA (tracrRNA). The following crRNAs were used: Dsp, 5′-CGTGATCACCGACCAAGAACT-3′; Pg, 5′-CATGGCCTCCCGCACCCGTT-3′; Pkp2, 5′-CGGCTACATCCGGACCGTCC-3′; Pkp3, 5′-GAAACCTGTCTCGGAACGCT-3′; and Par3, 5′-CCGGGTCCGTCCGAAGCACA-3′. The KO cell clones (at least three for each gene) were then selected through cloning, immunofluorescence, and verified by Western blotting. All independently obtained cell lines lacking a particular protein exhibited the same phenotype.

RNA-seq

About 1 1/2 million frozen DLD1 cells were sent to ACGT, Inc. (Wheeling, IL), which performed RNA-Seq analysis of the sample according to the company protocol. In brief, extracted RNA was used for constructing uniquely barcoded sequencing library using the NEXTflex Rapid mRNA-Seq Kit. The library was evaluated by Qubit and 2100 bioanalyzer and sequenced using the Illumina NextSeq flow cell. Bcl2fastq was used to demultiplex over 147 million paired end reads. Adapters, low-quality sequences (<Q30), and short reads (< 50 bp) were trimmed and filtered out using Trim Galore. The trimmed reads were mapped and aligned to the human genome using STAR aligner. Standard GATK guidelines were used to identify transcription variants and final reads were annotated and counted using GATK HaplotypeCaller and VCFtools vcf-annotate utility. The end product obtained from ACGT, Inc was a chart presenting relative expression of each transcript presented as a FPKM value (fragments per kilobase of transcript per million mapped reads).

Immunofluorescence microscopy

For widefield immunofluorescence, cells were cultured on glass coverslips for 48–64 h. The cells were fixed with 2% formaldehyde (10 min) and then permeabilized with 1% Triton X-100 and stained for corresponding antibodies (see Indra *et al.*, 2013 for details). The images were taken using an Eclipse 80i Nikon widefield microscope (objective lenses: Plan Apo 100× 1.40 NA; Figures 4B, 5F, 6, and 7; MARVELD-2 staining; Figure 8D; Supplemental Figures S1C, S2, S3, and S4G; and Plan Apo 40× 1.0; Figure 1A and Supplemental Figure S4A) and a digital camera (CoolSNAP HQ2; Photometrics). For confocal microscopy, the cells were cultured 48–64 h on glass-bottom dishes (P35G-1.5; MatTek) and fixed as described above if not specifically indicated. Immediately before imaging, the dishes were filled with 87% glycerol. The images were taken using a Nikon A1 laser scanning confocal microscope (Z step size was 0.5 µm in all cases) equipped with a Plan Apo TIRF 100× 1.45 NA objective lens. To image the surface-located Dsg2, the cells on the coverslips were incubated with anti-Dsg2 ectodomain antibody (PA5-21444; Invitrogen) for 30 min on ice. Then the cells were washed with the culture media and stained as described above.

The following antibodies were used: guinea pig anti-Dsp and anti-cingulin (DP-1 and GP26; Progen); goat anti-occludin antibody (sc-8145, Santa Cruz Biotechnology); rabbit antibodies: anti-Scrib and anti-Llgl1 (ab36708 and ab18302; Abcam), anti-ZO1, anti-MARVELD-2, anti-Par3, anti-β-catenin (40-2200, 700191, PA5-56475, MA5-14461, Invitrogen); anti-Dsg2 (21880-1-AP, Proteintech), anti-vinculin (SAB5500192, Sigma); mouse antibodies: anti-Pkp2 (651101S, Progen); anti-E-cadherin (clone HECD1; Zymed Laboratories); anti-GFP, anti-Pals1, anti-Pkp3 (sc-9996, sc-365411, sc-166655, correspondingly; Santa Cruz Biotechnology). Specificity of all these antibodies, except anti-GFP and MARVELD-2, was tested by a combination of Western blotting and specific CRISPR/Cas9 KO. All secondary antibodies were produced in Donkey (Jackson ImmunoResearch Laboratories).

In situ PLA

Cells were fixed and permeabilized as indicated above and incubated for 30 min with the indicated rabbit antibody and mouse monoclonal anti-Pkp3 antibody (Santa Cruz). Ligation and amplification were performed as described in the manufacturer's protocol (Duolink PLA; Sigma-Aldrich) using the following reagents: PLA probe anti–rabbit plus, PLA probe anti–mouse minus, and detection reagent Red. After PLA, the samples were incubated for additional 30 min with FITC-labeled donkey antibody against rabbit IgG.

Image processing

The images were processed and analyzed using Nikon's NIS-Elements version 5.02 platform. All sets were equally adjusted for all samples. For obtaining the apicobasal DSM plots, confocal images (representing 50 µm × 50 µm squares of cell culture) that are representative of three independent experiments were used. Background subtraction was done using a constant value of 400 for all frames that removed most of the non-DSM membrane staining. All images were then converted to 2D "Volume View" in which the *x*-axis represented X-Y grids drawn with same density as Z-stacks (0.5 µm). The *y*-axis represented the *z*-axis of the original image. This measurement quantifies the number of grids (0.5 × 0.5 µm) within each confocal slice for which fluorescence exceeds the selected threshold (number of DSMs) and the fluorescence intensity of each of these grids (intensity of DSMs). The result was transferred to Microsoft excel to plot the chart.

Quantification of the apical to cytosolic Dsg2 fluorescence ratio in WT and Pkp2/3-KO DLD1 cells was obtained using a total fluorescence of the 5 µm × 5 µm squares taken from the confocal slices of the apical membrane versus that of the identical squares taken from slices crossing the cytosol of the same cells. Ten ratios obtained for each of three experiments were used to determine three independent averages, which were then used for plotting the graphs and for statistics. The PCC were determined based on entire images (containing about 8–10 cells each) or separately for tC and bC contacts taken by the 100× objectives using either widefield or confocal microscopes. Four images from each of three independent experiments were analyzed for total PCC. The same images were used for PCC analyses of the bC and tC contacts (10 contacts of each type for each of the experiments). Three averages determined for each of the experiment were then used in the graphs. The PLA signals were selected by a thresholding function and the number of particles was counted by an object-counting function. All PCC values were measured after subtraction of background fluorescence (based on cytosolic fluorescence). Three independent experiments were performed for each PLA. Four independent images from each of them were used for quantification of total PLA signals and 15 bC and tC contacts were quantified within each group. All graphs, chards, error bars, and statistics were plotted using GraphPad Prism 9.1.1.225. Quantitative data are presented as the mean and SE. Statistical significance was analyzed using the Student's two-tailed *t* test for two groups and ANOVA analysis for more groups. Corresponding *p* values are indicated in the figure legends.

ACKNOWLEDGMENTS

Sequencing, flow cytometry, and confocal microscopy were performed at the Northwestern University Genetic, Flow Cytometry,

and Advanced Microscopy Centers. The authors declare no competing financial interests. The work was supported by grants from the National Institutes of Health: AR44016 and AR070166 (to S.M.T.), and R37AR043380 and R01AR041836 (to K.J.G.).

REFERENCES

Abe K, Takeichi M (2008). EPLIN mediates linkage of the cadherin catenin complex to F-actin and stabilizes the circumferential actin belt. Proc Natl Acad Sci USA 105, 13–19.

Badu-Nkansah KA, Lechler T (2020). Proteomic analysis of desmosomes reveals novel components required for epidermal integrity. Mol Biol Cell 31, 1140–1153.

Bär J, Kumar V, Roth W, Schwarz N, Richter M, Leube RE, Magin TM (2014). Skin fragility and impaired desmosomal adhesion in mice lacking all keratins. J Invest Dermatol 134, 1012–1022.

Bonello TT, Peifer M (2019). Scribble: A master scaffold in polarity, adhesion, synaptogenesis, and proliferation. J Cell Biol 218, 742–756.

Bonné S, Gilbert B, Hatzfeld M, Chen X, Green KJ, van Roy F (2003). Defining desmosomal plakophilin-3 interactions J Cell Biol 161, 403–416.

Brasch J, Harrison OJ, Honig B, Shapiro L (2012). Thinking outside the cell: how cadherins drive adhesion. Trends Cell Biol 22, 299–310.

Broussard JA, Getsios S, Green KJ (2015). Desmosome regulation and signaling in disease. Cell Tissue Res 360, 501–512.

Campbell HK, Maiers JL, DeMali KA (2017). Interplay between tight junctions & adherens junctions. Exp Cell Res 358, 39–44.

Chen X, Bonne S, Hatzfeld M, van Roy F, Green KJ (2002). Protein binding and functional characterization of plakophilin 2. Evidence for its diverse roles in desmosomes and beta -catenin signaling. J Biol Chem 277, 10512–10522.

Chen X, Macara IG (2005). Par-3 controls tight junction assembly through the Rac exchange factor Tiam1. Nat Cell Biol 7, 262–269.

Choi J, Troyanovsky RB, Indra I, Mitchell BJ, Troyanovsky SM (2019). Scribble, Erbin, and Lano redundantly regulate epithelial polarity and apical adhesion complex. J Cell Biol 218, 2277–2293.

Dow LE, Humbert PO (2007). Polarity regulators and the control of epithelial architecture, cell migration, and tumorigenesis. Int Rev Cytol 262, 253–302.

Farquhar MG, Palade GE (1963). Junctional complexes in various epithelia. J Cell Biol 17, 375–412.

Fuchs M, Foresti M, Radeva MY, Kugelmann D, Keil R, Hatzfeld M, Spindler V, Waschke J, Vielmuth F (2019). Plakophilin 1 but not plakophilin 3 regulates desmoglein clustering. Cell Mol Life Sci 76, 3465–3476.

Fujiwara M, Nagatomo A, Tsuda M, Obata S, Sakuma T, Yamamoto T, Suzuki ST (2015). Desmocollin-2 alone forms functional desmosomal plaques, with the plaque formation requiring the juxtamembrane region and plakophilins. J Biochem 158, 339–353.

Garcia MA, Nelson WJ, Chavez N (2018). Cell-cell junctions organize structural and signaling networks. Cold Spring Harb Perspect Biol 10, a029181.

Gerull B, Heuser A, Wichter T, Paul M, Basson CT, McDermott DA, Lerman BB, Markowitz SM, Ellinor PT, MacRae CA, *et al.* (2004). Mutations in the desmosomal protein plakophilin-2 are common in arrhythmogenic right ventricular cardiomyopathy. Nat Genet 36, 1162.

Godsel LM, Dubash AD, Bass-Zubek AE, Amargo EV, Klessner JL, Hobbs RP, Chen X, Green KJ (2010). Plakophilin 2 couples actomyosin remodeling to desmosomal plaque assembly via RhoA. Mol Biol Cell 21, 2844–2859.

Goldstein B, Macara IG (2007). The PAR proteins: fundamental players in animal cell polarization. Dev Cell 13, 609–622.

Green KJ, Getsios S, Troyanovsky S, Godsel L (2010). Intercellular junction assembly, dynamics, and homeostasis. Cold Spring Harb Perspect Biol 2, a000125.

Harris TJC (2017). Protein clustering for cell polarity: Par-3 as a paradigm. F1000Res 6, 1620.

Harrison OJ, Brasch J, Lasso G, Katsamba PS, Ahlsen G, Honig B, Shapiro L (2016). Structural basis of adhesive binding by desmocollins and desmogleins. Proc Natl Acad Sci USA 113, 7160–7165.

Hatzfeld M, Wolf A, Keil R (2014). Plakophilins in desmosomal adhesion and signaling. Cell Commun Adhes 21, 25–42.

Hirose T, Izumi Y, Nagashima Y, Tamai-Nagai Y, Kurihara H, Sakai T, Suzuki Y, Yamanaka T, Suzuki A, Mizuno K, *et al.* (2002). Involvement of ASIP/PAR-3 in the promotion of epithelial tight junction formation. J Cell Sci 115, 2485–2495.

Hofmann I (2020). Plakophilins and their roles in diseased states. Cell Tissue Res 379, 5–12.

Holthöfer B, Windoffer R, Troyanovsky S, Leube RE (2007). Structure and function of desmosomes. Int Rev Cytol 264, 65–163.

Humbert PO, Dow LE, Russell SM (2006). The Scribble and Par complexes in polarity and migration: friends or foes? Trends Cell Biol 16, 622–630.

Imamura Y, Itoh M, Maeno Y, Tsukita S, Nagafuchi A (1999). Functional domains of α-catenin required for the strong state of cadherin-based cell adhesion. J Cell Biol 144, 1311–1322.

Indra I, Hong S, Troyanovsky R, Kormos B, Troyanovsky S (2013). The adherens junction: a mosaic of cadherin and nectin clusters bundled by actin filaments. J Invest Dermatol 133, 2546–2554.

Joberty G, Petersen C, Gao L, Macara IG 2000. The cell-polarity protein Par6 links Par3 and atypical protein kinase C to Cdc42. Nat Cell Biol 2, 531–539.

Keil R, Rietscher K, Hatzfeld M (2016). Antagonistic regulation of intercellular cohesion by Plakophilins 1 and 3. J Invest Dermatol 136, 2022–2029.

Koeser J, Troyanovsky SM, Grund C, Franke WW (2003). De novo formation of desmosomes in cultured cells on transfection of genes encoding specific desmosomal components. Exp Cell Res 285, 114–130.

Moch M, Schwarz N, Windoffer R, Leube RE (2020). The keratin–desmosome scaffold: pivotal role of desmosomes for keratin network morphogenesis. Cell Mol Life Sci 77, 543–558.

Ozawa M (1998). Identification of the region of α-catenin that plays an essential role in cadherin-mediated cell adhesion. J Biol Chem 273, 29524–29529.

Rietscher K, Keil R, Jordan A, Hatzfeld M (2018). 14-3-3 proteins regulate desmosomal adhesion via plakophilins. J Cell Sci 131, jcs212191.

Roberts BJ, Johnson KE, McGuinn KP, Saowapa J, Svoboda RA, Mahoney MG, Johnson KR, Wahl JK 3rd (2014). Palmitoylation of plakophilin is required for desmosome assembly. J Cell Sci 127, 3782–3793.

Rübsam M, Broussard JA, Wickström SA, Nekrasova O, Green KJ, Niessen CM (2018). Adherens junctions and desmosomes coordinate mechanics and signaling to orchestrate tissue morphogenesis and function: an evolutionary perspective. Cold Spring Harb Perspect Biol 10, a029207.

Shafraz O, Rübsam M, Stahley SN, Caldara AL, Kowalczyk AP, Niessen CM, Sivasankar S (2018). E-cadherin binds to desmoglein to facilitate desmosome assembly. Elife 7, e37629.

Sumigray KD, Lechler T (2012). Desmoplakin controls microvilli length but not cell adhesion or keratin organization in the intestinal epithelium. Mol Biol Cell 23, 792–799.

Tepass U, Tanentzapf G, Ward R, Fehon R (2001). Epithelial cell polarity and cell junctions in Drosophila. Annu Rev Genet 35, 747–784.

Todorovic V, Koetsier JL, Godsel LM, Green KJ (2014). Plakophilin 3 mediates Rap1-dependent desmosome assembly and adherens junction maturation. Mol Biol Cell 25, 3749–3764.

Troyanovsky SM, Troyanovsky RB, Eshkind LG, Leube RE, Franke WW (1994). Identification of amino acid sequence motifs in desmocollin, a desmosomal glycoprotein, that are required for plakoglobin binding and plaque formation. Proc Natl Acad Sci USA 91, 10790–10794.

Troyanovsky S (2012). Adherens junction assembly. Subcell Biochem 60, 89–108.

Vasioukhin V, Bowers E, Bauer C, Degenstein L, Fuchs E (2001). Desmoplakin is essential in epidermal sheet formation. Nat Cell Biol 3, 1076–1085.